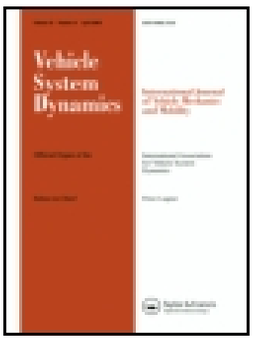

Taylor & Francis
Taylor & Francis Group

Vehicle System Dynamics
International Journal of Vehicle Mechanics and Mobility

ISSN: 0042-3114 (Print) 1744-5159 (Online) Journal homepage: http://www.tandfonline.com/loi/nvsd20

Real-time characterisation of driver steering behaviour

Matthew C. Best

To cite this article: Matthew C. Best (2018): Real-time characterisation of driver steering behaviour, Vehicle System Dynamics, DOI: 10.1080/00423114.2018.1447678

To link to this article: https://doi.org/10.1080/00423114.2018.1447678

Published online: 16 Mar 2018.

VEHICLE SYSTEM DYNAMICS, 2018
https://doi.org/10.1080/00423114.2018.1447678

Real-time characterisation of driver steering behaviour

Matthew C. Best

Department of Aeronautical and Automotive Engineering, Loughborough University, Loughborough, UK

ABSTRACT

In recent years the application of driver steering models has extended from the off-line simulation environment to autonomous vehicles research and the support of driver assistance systems. For these new environments there is a need for the model to be adaptive in real time, so the supporting vehicle systems can react to changes in the driver, their driving style, mood and skill. This paper provides a novel means to meet these needs by combining a simple driver model with a single-track vehicle handling model in a parameter estimating filter – in this case, an unscented Kalman filter. Although the steering model is simple, a motion simulator study shows it is capable of characterising a range of driving styles and may also indicate the level of skill of the driver. The resulting filter is also efficient – comfortably operating faster than real time – and it requires only steer and speed measurements from the vehicle in addition to the reference path. Adaptation of the steer model parameters is demonstrated along with robustness of the filter to errors in initial conditions, using data from five test drivers in vehicle tests carried out on the open road.

Abbreviations: ADAS: advanced driver assistance systems; CG: centre of gravity; CAN: controller area network; EKF: extended Kalman filter; GPS: global positioning system; UKF: unscented Kalman filter

ARTICLE HISTORY
Received 4 July 2017
Revised 11 December 2017
Accepted 23 February 2018

KEYWORDS
Driver behaviour; driver–vehicle systems; driver assistance systems; system identification; parameter estimation

Nomenclature

Vehicle and driver models

a, b	front, rear axle distances from vehicle CG (m)
C_α	tyre cornering stiffness (N/rad)
d	signed deviation of projected vehicle path (P) from the reference path (m)
g	gravitational acceleration (m/s^2)
$\boldsymbol{G}$	global CG position vector
i	index number of current line segment
I_{zz}	yaw inertia (kg m^2)
K_{ug}	understeer gradient perceived by driver (rad)
K_{lat}	proportional steering control feedback gain (rad/m)
L	vehicle wheelbase (m)

CONTACT Matthew C. Best m.c.best@lboro.ac.uk

M	vehicle mass (kg)
$\mathbf{n_L}$	normal to reference path line segment vector (see $\mathbf{r_L}$)
$\mathbf{P}$	global projected CG position vector
r	yaw angular velocity (rad/s)
$\mathbf{r_L}$	reference path line segment vector ($\mathbf{E_L} - \mathbf{S_L}$)
R	radius of projected vehicle path (m)
$\mathbf{S_L}, \mathbf{E_L}$	start, end points of reference path line segment
$\hat{\mathbf{t}}_\mathbf{G}, \hat{\mathbf{n}}_\mathbf{G}$	unit vector tangential, normal to vehicle orientation
u	longitudinal velocity (m/s)
v	lateral velocity (m/s)
X, Y	global position of vehicle CG (m)
δ	steered wheel angle (rad)
μ	friction coefficient (–)
θ	angle of projected vehicle path (rad)
ψ	yaw angle (rad)

Kalman filter

$\mathbf{f}$	system model of state derivatives
$\mathbf{h}$	model of outputs
$\mathbf{K}$	Kalman gain matrix
n	number of states
$\mathbf{P}$	state error covariance matrix
$\mathbf{P}_{xy}$	state-output cross-correlation matrix
$\mathbf{P}_{yy}$	output error covariance matrix
$\mathbf{Q}$	model error covariance matrix
$\mathbf{R}$	output (measurement) covariance matrix
T	discrete time step duration (s)
$\mathbf{u}$	input vector
W	weighting applied to the sigma points
$\mathbf{x}$	state vector
$\mathbf{y}$	output (measurement) vector
$\mathbf{z}$	combined state and parameter vector
κ	UKF weighting parameter
θ	parameters vector
ρ	UKF tuning parameter, affecting speed of variation of adapted parameters
υ	vector of errors between modelled and measured outputs
ω	vector of state propagation and modelling errors
Υ	output estimate generated from sigma points
χ	sigma point – disturbed state vector used to numerically estimate covariances

Qualifications

f, r	front, rear
k	time step
L	relating to a specific line segment

* intermediate update of vector/matrix
$\hat{}$ optimal estimate (Kalman filter)/unit length vector (driver model)

1. Introduction

Driver models were originally devised for the simulation environment, to enable closed-loop simulation and explore driver–vehicle dynamic interactions. Early research achieved effective path following control by minimising error at multiple preview ('lookahead') points on the road; the most popular by MacAdam [1] has become the de-facto standard. Sharp et al. [2] then combined multiple reference points with yaw rate feedback in an optimal controller, and Ungoren and Peng [3] considered a similar approach; Ungoren and Peng [3] also provide a useful literature review of the period.

In recent years the applications for driver modelling have increased to support advanced driver assistance systems (ADAS) and autonomous vehicle research. With these, the focus has shifted away from the mechanistic path following task toward a better understanding and replication of the full driver dynamic system. Keen and Cole first extended the concept of multi-point preview, adding an internal model and optimising future steer trajectory using model predictive control in [4]. Cole then highlighted the importance of modelling the driver's neuromuscular dynamics in [5] – an issue also recognised by Bi et al. in [6] and developed by Flad et al. in [7]. Most recently, Nash and Cole [8] extended the biomechanical analysis to model sensory organs; significant effort has gone into matching individual test driver response using these multi-parameter models.

An obvious and important outcome of such studies is the correlation between model parameters and driver awareness and skill. Alertness was investigated in Saigo et al. [9] and multiple levels of skill were proposed in Erseus et al. [10]. Moon and Seibum [11] achieved impressive averaged results using a complex model including variable preview and neuromuscular system with around 30 parameters set to match four skill levels. However, a common limitation of all of these papers is their use of an emergency manoeuvre to do the fitting – a double-lane change in [10–12] and the Elk test in [5], and their restriction to the use of vehicle simulators for obvious safety reasons. The best test of a driver's skill is certainly their behaviour in an emergency scenario, yet almost 100% of all driving experience for most drivers excludes emergencies. The gold standard would be to deduce driver skill from normal driving in advance of an emergency, and also to take note of the variations in awareness and skill which most drivers experience over time – often within single journeys.

Driver behaviour can also be categorised more widely, using subjective data usually obtained via questionnaire; e.g. in [13] Ostapczuk et al. validate self-reported data that correlate average speed and driving experience with the number of accidents. It is possible to identify individual drivers from their driving style, e.g. by using long-term records of mean and peak accelerations in [14]. However, it is more challenging to accurately relate the changing psychological state of the driver to measurables; in [15], Carmona et al. attempt to detect aggressive vs. 'normal' driving using an expert system, though this relies on some arbitrary setting of acceptable acceleration range, and on drivers being asked to drive 'in an aggressive way' – a process unlikely to be realistic. Chu et al. come closest to relating cautious, moderate and aggressive driver states to a set of five objective speed, steer and

acceleration measures, in [16]. They use fuzzy sets and also make appropriate correlations to a separate self-reported questionnaire on temperament.

Systematic identification of driver behaviour from driving data is rare in the literature. Tokutake et al. achieved some success, particularly in rejection of unmodelled steer disturbances in [17], though again with restricted paths and mostly through simulation. Interestingly, they adopt a simpler structure of driver model than most, which is essential to support well-determined parameter identification. Papers with a similar focus include identification of driver delay by Hosseini et al. [18] and identification of a simple second order model by Mihaly and Gaspar [19]. Neither of these considers real-time adaptation which would also be needed to adapt to driver changes, though [18] uses least-squares identification which could be made recursive.

This paper attempts to address many of the weaknesses of recent studies. Here, we consider normal driving on the open road in addition to the correlation of normal driving and emergency manoeuvres on a vehicle simulator. Further, the driver/vehicle model is coupled with a real-time estimator, capable of operating in current vehicles as it uses only steer and forward speed measurements. The necessary concession is a simplification of the driver model itself. However the expectation is that a simple model with adapted parameters may be capable of replicating the performance of more complex bio-realistic fixed parameter models, while also capturing real-time variations in driver behaviour.

The simple realistic driver model considered here was originally published in Best [20], motivated by the author's perhaps contentious belief that the driving task actually uses single point preview. It is unlikely that everyday driving involves multi-point weighted calculations in real time; rather, the driver continuously tracks a section of the road ahead, and drives to it. An interesting paper on intermittent attention and response by Johns and Cole [21] suggests that there is scope for the obviously wider attention to the environment which the driving task involves. The lookahead point surely varies as we drive, due to speed and other factors, but the proposed model is demonstrated to be capable of matching measured steer behaviour in a range of scenarios.

2. A simple realistic lateral driver model

A particular problem with driver modelling is an accurate but computationally simple representation of the road. Smooth, e.g. circular or splined road segments provide a continuous reference, but these need to be fitted to known physical roads that are usually available as a trace of coordinates. Here we use the simplest road reference directly, linearly interpolating a set of coordinates, though if required, this driver model method also lends itself well to implementation on circular road segments [20].

Figure 1 illustrates the basic premise of this single preview point method, which assumes the driver retains a continuous understanding of the simple circular (steady-state) path that the car will follow if the current steer angle is maintained. The driver's internal model is thus assumed to be restricted to a basic (though possibly time-varying) understanding of steering gain. The model evaluates signed lateral error of the single preview point **P**, which is located by projecting along the current circular arc.

The control operates discretely, from the known global CG position of the vehicle, **G**, yaw angle ψ, speed u and steered wheel angle δ at time step k. The forward path radius

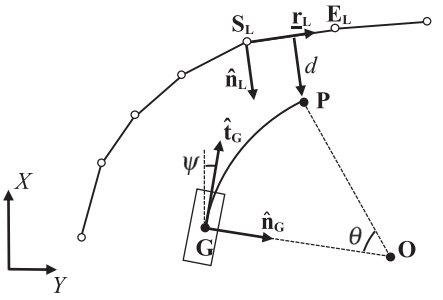

Figure 1. Calculation of preview point and lateral deviation from line segment track.

under fixed steer angle and constant speed is, from the well-known steady-state handling equation [22],

$$R_k = \frac{L + K_{ug} u_k^2 / g}{\delta_{k-1}}. \tag{1}$$

Unit vectors are then found by rotation of the global X facing vector through ψ

$$\hat{\mathbf{t}}_\mathbf{G} = \begin{pmatrix} \cos\psi \\ \sin\psi \end{pmatrix}, \hat{\mathbf{n}}_\mathbf{G} = \begin{pmatrix} -\sin\psi \\ \cos\psi \end{pmatrix} \tag{2}$$

and the angle traversed along the arc depends on preview time T_p,

$$\theta = \frac{u_k T_p}{R_k}. \tag{3}$$

A convenient way to locate point **P** is via the arc centre **O**,

$$\mathbf{P} = \mathbf{G} + R\hat{\mathbf{n}}_\mathbf{G} - \begin{pmatrix} \cos\theta & -\sin\theta \\ \sin\theta & \cos\theta \end{pmatrix} R\hat{\mathbf{n}}_\mathbf{G}. \tag{4}$$

The signed deviation from a given linear segment of track is then

$$d = (\mathbf{P} - \mathbf{S}_\mathbf{L}) \cdot \hat{\mathbf{n}}_\mathbf{L}, \tag{5}$$

where, for the segment to be valid,

$$0 < (\mathbf{P} - \mathbf{S}_\mathbf{L}) \cdot \hat{\mathbf{r}}_\mathbf{L} < |\mathbf{r}_\mathbf{L}|. \tag{6}$$

Here, the smallest valid d will be appropriate, but two snags arise in that (a) checking all segments is computationally expensive and (b) since the line segment track is strictly discontinuous in gradient, conditions can arise where two, or zero valid segments exist. To avoid both problems, we take advantage of the fact that **P** will only progress forward along the track, so the track segment index i can only stay the same or increase. At each new discrete step, the track segment is carried over, $i_k = i_{k-1}$ and incremented as required

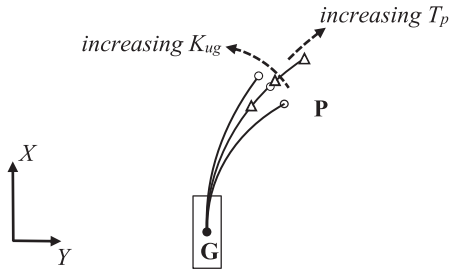

Figure 2. Effect of parameter variation on projected path point **P.**

according to

$$\text{while } (\mathbf{P} - \mathbf{S_L}(i_k)) \cdot \hat{\mathbf{r}}_\mathbf{L}(i_k) > |\mathbf{r_L}(i_k)|, \quad i_k = i_k + 1. \tag{7}$$

Steering control is then based solely on correction of the current steer value, given the predicted future point error d. This is applied using a proportional gain K_{lat}

$$\delta_{k+1} = \delta_k - K_{lat} d. \tag{8}$$

Although it is very simple, this steering model is realistic, effective, computationally efficient and tunable through variation of just a few parameters; code for implementing it in Matlab/Simulink is provided in the Appendix.

Considering Equation (1), the radius of the expected future path of the vehicle is determined for a given steering angle and speed, by wheelbase L and understeer gradient K_{ug}. Accepting L as fixed we can use K_{ug} as a driver model parameter which represents the driver's estimate of steering gain. Figure 2 illustrates this, using circle markers to show how **P** varies with increasing K_{ug}; higher values decrease the expected radius, reducing the steering gain. An expert driver might be capable of continuously matching their perceived K_{ug} to the actual vehicle understeer gradient (if we ignore modelling errors and assume purely steady-state manoeuvres) but a less skilled driver's estimate may be less accurate and/or vary with concentration level. K_{ug} can therefore be usefully tuned to reflect the driver's tendency to under/overcompensate their changes in steering through and after corners.

Lookahead time T_p is also clearly a useful characterising parameter; its effect on **P** is illustrated in Figure 2 with triangle markers, with increasing T_p causing longer lookahead distance. This affects the phasing of the steer input, as higher T_p causes steer actions to be applied earlier for a given corner. When coupled with the controller, higher T_p induces lower magnitude steer inputs which are held for a longer duration, inducing corner cutting, whereas low T_p causes higher magnitude, shorter duration steer inputs. Although K_{ug} and T_p are not exactly orthogonal in their effect, they have distinctly different effects on the controlled response and we will see they can be usefully adapted simultaneously.

Finally, the proportional feedback gain K_{lat} could also be tuned, but its influence on steering behaviour is strongly coupled to K_{ug}; they both affect the strength of feedback to lateral deviation error. Setting K_{lat} anywhere between 10^{-4} and 0.5 provides stable results over a wide range of settings of K_{ug} and T_p at the 100 Hz sampling rate used here, so independent tuning is also not useful; indeed, adaptation can lead to instability. We therefore fix the feedback gain at $K_{lat} = 0.001$.

3. Model application and parameter optimisation

In [20], a range of parameter combinations was shown to provide robust lane tracking on a simulated lane-change manoeuvre at both low and high speeds, so here we move directly to the application of the model in comparison to, and replication of, real steer behaviour from driver tests. Two test environments have been considered – a motion-base driving simulator and driving on the public road.

Simulated driving took place on an electrically driven Cruden™ Stewart platform, with motion cueing tuned specifically for automotive testing. This is known to provide an immersive simulation environment with realistic motion cues and minimal incidence of simulator sickness [23] – see Figure 3. A fully representative 14 dof vehicle model employing combined-slip Pacejka tyres was configured to represent a D-class saloon car with automatic gearbox. Test drives were conducted on a fictional, dry, empty single carriageway road with a fairly generous (4.5 m) lane width offering a range of corner curvatures as well as some modest vertical variation (Figure 3). Drivers were told to drive as they would on a public highway in the presence of oncoming traffic, and were given one trial lap of the test track (taking approximately 10 min) to acclimatise to the simulator and rehearse the speed they wished to drive at. The freedom to adjust driving speed as you wish is an important factor in simulating real-world response and in testing the driver model; since driving simulators can give a false impression of speed, the drivers were not given sight of the speedometer. Any driver who strayed out of the lane on the test lap would have been disqualified, though this was not necessary in practice and a good range of speeds was observed across the five drivers who were examined. A profile of the drivers is given in Table 1. Of course with such a small set of drivers, all of which are male, some driving styles may not be represented and it will not be possible to make statistically rigorous statements about driving behaviour. However, we will see significant differences in driving skill, steer and speed preference between the drivers, which allow adequate demonstration of the new method.

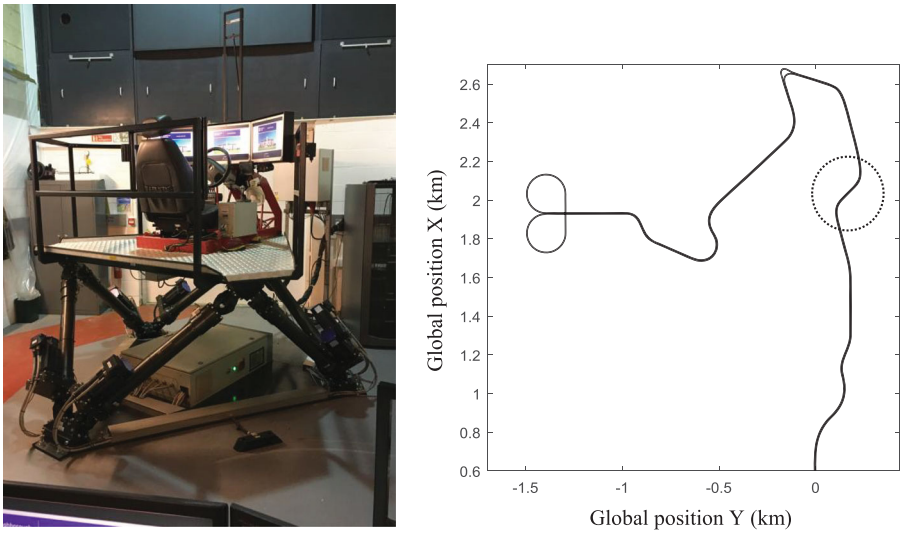

Figure 3. Motion simulator (left) and simulated path (right).

Table 1. Test driver profiles.

Driver	Sex	Age	Occupation	Years driving experience	Hours driving per week	Own car (gearbox)
B	M	49	Lecturer	31	1	Ford Galaxy (manual)
C	M	25	Ph.D. student	8	10	BMW 323i (auto)
F	M	48	IT manager	26	9	Mitsubishi Colt (manual)
K	M	29	Lecturer	11	3	Jaguar XF (auto)
T	M	38	Experimental officer	21	12	Volvo V50 (manual)

The same five drivers also drove a 60-km circuit of public B class roads in Leicestershire, UK, between Loughborough and Melton Mowbray, on a dry, clear day in a Jaguar XE automatic instrumented with an OXTS™ inertial navigation system recording accurate GPS position, vehicle speed, lateral acceleration and with separate simultaneous recordings of the steering wheel angle from the vehicle CAN. Manufacturer supplied steering geometry then enabled calibration to establish steered wheel angle. The drivers were again instructed to drive freely at self-regulated speed, and sections of data were recorded only on de-restricted sections of road with no vehicle in front. A separate traverse of the circuit was conducted at a fixed speed of 40 kph with the test vehicle strictly maintained in the centre of the lane, in order to establish a reference path for the driver model.

First, consider some interesting detail from the test data (Figure 4). On the open road, the drivers self-regulated their speed such that lateral accelerations did not exceed 4 m/s^2 (plot b) despite choosing a range of cruise speeds on straights (plot a). Of course, slowing down for corners is a necessary evil(!) but the consistent choice of 4 m/s^2 as maximum lateral acceleration from all drivers independently is interesting. Maximum accelerations on the simulator were a little higher, at 5.5 m/s^2 but this is to be expected given the significantly reduced lateral force feedback available there. It is recognised that motion simulators provide compromised vestibular feedback to the driver and care should be taken not to over-infer from simulator tests alone. In these tests of normal driving, with lower magnitude vehicle excitation, the visual feedback dominates [23], so the vehicle response feels reasonably natural. We should not expect metrics from simulated vs. road tests to be identical, but can be encouraged by the similarity in overall behaviour.

We see further evidence that the simulator invokes a naturalistic response in another interesting detail of Figure 4 where steer traces on straight sections of road are shown, for the road tests (plot c) and simulator tests (plot d). In both scenarios, all drivers exhibit an inconsistent 'steer hunting' behaviour, continuously varying the steering indeterministically. They are allowing steer to vary around zero rather than fixing $\delta = 0$ as we might expect, and as driver models will generally behave. The same driver behaviour is seen, to a lesser extent, on steady-state corners (not shown). We might expect this behaviour to be caused by vertical vibrations from the road surface; indeed, this may account for higher frequency content in plot (c). However, local road disturbances are absent on the simulator, yet the steer hunting phenomenon is still clear. The presence of friction and damping in the steering system might also have an effect, but again these parameters vary between the test vehicle and simulator, with the simulator having negligible friction or damping. Interestingly, there is broad consistency between the simulator and road experiments in steer

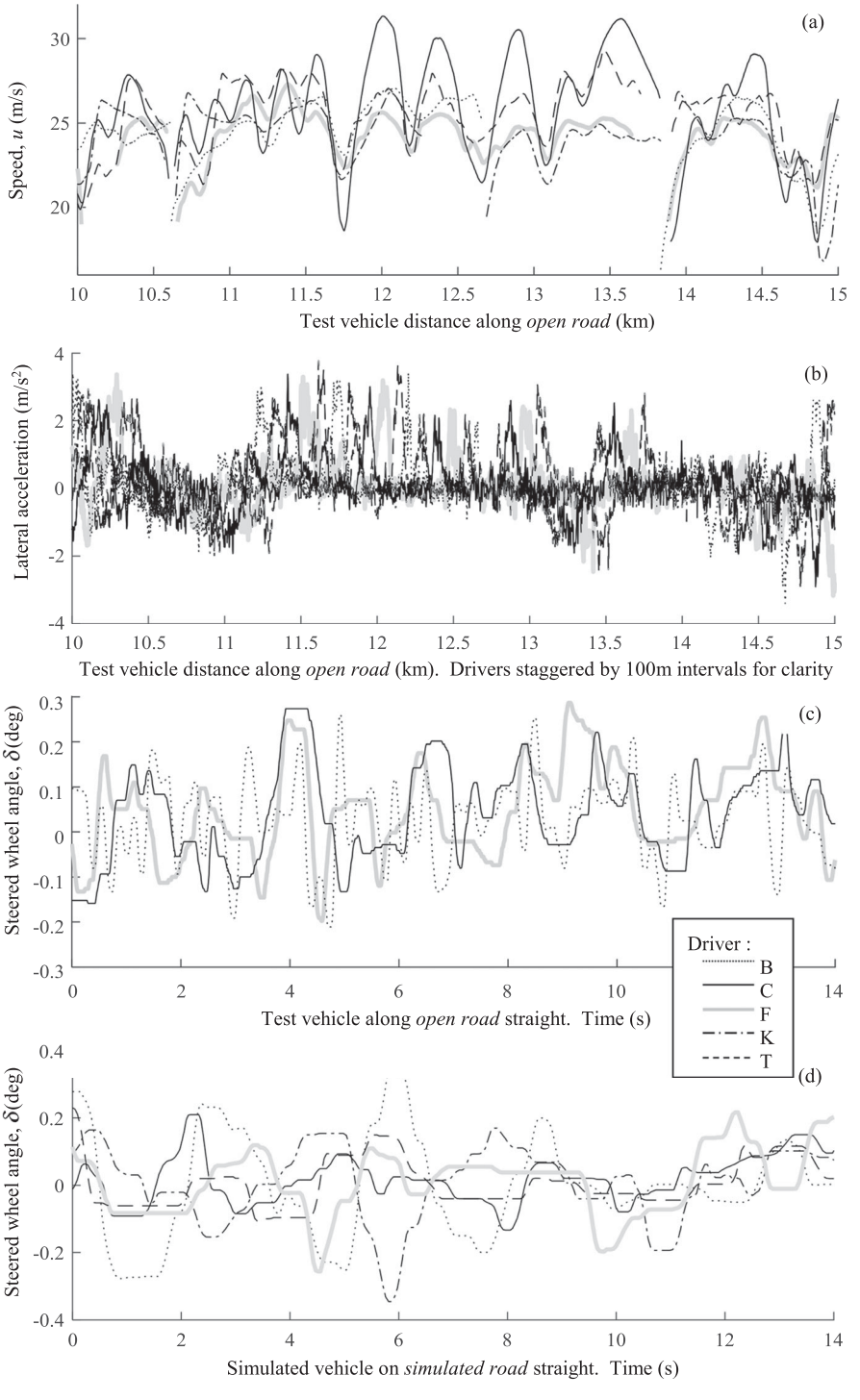

Figure 4. Generic driver metrics.

Table 2. Handling model parameters.

	M (kg)	I_{zz} (kg m^2)	$C_{\alpha f}$ (kN/rad)	$C_{\alpha r}$ (kN/rad)	a (m)	b (m)
Simulator	1630	3200	107	92	1.18	1.57
Test vehicle	1855	3600	84	93	1.40	1.55

amplitudes, with both peaking around 0.3° (4.5° at the handwheel). Frequencies broadly vary between 0.2 and 2 Hz, with the higher frequency content only seen in the test vehicle. There is no time correlation or consistency to the behaviour, even for any individual driver, so it will not be possible for a driver model to explain systematically; we must treat it as a significant source of noise when considering the accuracy of fit between modelled and measured steer.

To test and tune the driver model, it must be coupled with a vehicle model. Given the above linear driving behaviour, and in the interests of computational efficiency, a linear single-track model is sufficient (see, e.g. [22]). This has local axis system vehicle states for lateral velocity, yaw rate and angle, $\mathbf{x} = [v, r, \psi]^{\mathrm{T}}$

$$\dot{\mathbf{x}} = \begin{bmatrix} -(C_{\alpha f} + C_{\alpha r})\mu/(Mu) & (bC_{\alpha r} - aC_{\alpha f})\mu/(Mu) - u & 0 \\ (bC_{\alpha r} - aC_{\alpha f})\mu/(I_{zz}u) & -(a^2C_{\alpha f} + b^2C_{\alpha r})\mu/(I_{zz}u) & 0 \\ 0 & 1 & 0 \end{bmatrix} \mathbf{x} + \begin{bmatrix} C_{\alpha f}\mu/M \\ aC_{\alpha f}\mu/I_{zz} \\ 0 \end{bmatrix} \delta \tag{9}$$

and to provide CG position for the driver model, it is augmented with global states

$$\begin{pmatrix} \dot{X} \\ \dot{Y} \end{pmatrix} = \begin{bmatrix} \cos\psi & -\sin\psi \\ \sin\psi & \cos\psi \end{bmatrix} \begin{pmatrix} u \\ v \end{pmatrix}. \tag{10}$$

It is not necessary to match the vehicle model parameters exactly to the test vehicle or motion simulator model – only an approximate match of steering gain is required, so most parameters are set to nominally represent the simulated and test-driven D-class cars; $C_{\alpha r}$ is then approximately tuned in each case to give comparable steering gain (Table 2).

By providing an initial state which matches the test data, and with the measured speed time history $u(t)$ applied as a known input, the coupled driver–vehicle system of Equations (1)–(10) can be run as a semi-independent dynamic system. This produces steer values that closely match the test vehicle, without continuous knowledge of the actual test vehicle position. Further, the tunable parameters K_{ug} and T_p can be optimised to improve the steer fit.

Consider the range of driving behaviours seen over a pair of corners in the simulation study, annotated in Figure 3 (right); speed and steer traces for the five drivers are given in Figure 5(a,b). A Nelder–Meade simplex optimisation was conducted to optimise K_{ug} and T_p over the whole test circuit for each driver, and results for the two most extreme drivers are shown in Figure 5(c) with parameter settings in Table 3 (standard run).

Note in Figure 5(b) how drivers K and C employ lower magnitude steer into the first corner, how driver F has greater steer oscillation between corners and how the speeds vary considerably between the drivers. The optimised driver models for drivers C and F (plot c) show the level of accuracy the driver model is capable of. The tuned model cannot replicate the steer response exactly, partly as a result of the indeterministic steer hunting errors discussed earlier. But it does properly reflect the different characteristics of driving style, with

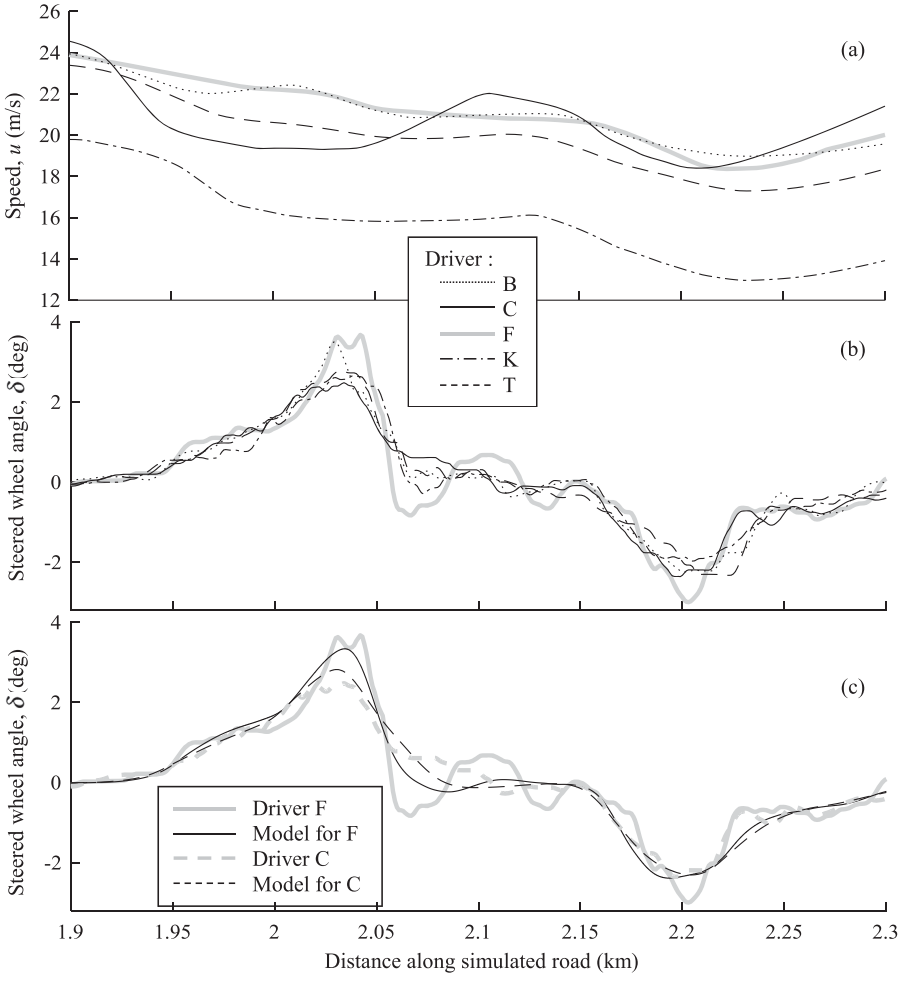

Figure 5. Driver characteristics and optimal model fit.

Table 3. Simulator test optimised models and skill metrics.

	Driver identifier				
	B	C	F	K	T
Standard run T_p (s), $K_{ug}/10^3$ (rad/g)	0.81, 0.3	0.92, 0.8	0.56, −1.3	0.97, −0.4	0.83, 0.1
First event run T_p (s), $K_{ug}/10^3$ (rad/g)	1.15, 2.3	1.34, 5.7	0.80, −0.1	1.63, 9.7	0.94, −0.3
Second event run T_p (s), $K_{ug}/10^3$ (rad/g)	1.15, 2.6	1.38, 6.1	1.05, 2.5	1.25, 3.8	1.16, 2.3
Number of loss of control events[a]	2	0	7	4	3
Average path error[b] (m)	0.52	0.37	0.74	0.53	0.45

[a]Events where the vehicle CG moved out of the lane.
[b]Average error from path centreline in 2 s following each event.

lower magnitude, longer and more smoothly varying steer behaviour for driver C and with higher peak and more oscillatory steer for driver F. These characteristics are also reflected in the parameters, where we see higher T_p for driver C and lower T_p coupled with low K_{ug} for driver F. Recall that we do not expect optimised K_{ug} to match the test vehicle; here it is

an independent steering gain metric within the closed-loop control, influencing steering correction behaviour.

A supplementary experiment on the motion simulator allows us to relate the basic driving behaviour captured in the model, to driving skill. After the standard run, drivers were asked to complete two more circuits during which disturbance events were introduced at random. These were simulated by a rapid reduction of the friction at both front or both rear wheels, from $\mu = 1$ to $\mu = 0.2$ for 10–20 m, at random positions on randomly selected corners. The random placement caused some of these events to be negligible to the driver, whereas others were significant enough to cause complete loss of control. Drivers were told to react to these 'emergencies' as if on the public road, but to forget each event and continue as normal, once re-established on the track.

Results for the reoptimised driver models are also given in Table 3. Note how these disturbances cause all drivers to adopt longer lookahead times T_p; a reasonable interpretation here is that the events cause the drivers to adopt greater caution (or take greater care) with their steering on average, and this leads to higher T_p. Note also that the relative magnitude of T_p between the drivers remains consistent, with F always lowest and C and K consistently highest.

Figure 6 shows what happens when the *standard* drive settings of K_{ug} and T_p are used to run the driver model; this is compared with the actual driver response on the first significant event, in the first event run, for drivers F and C. Standard tuned driver model F loses control with almost exactly the same steer reaction, at least initially, as driver F. The $-10°$ held steer at 2.1 km shows a typical driver reaction, to freeze the steering (over 50 m – around 2 s) after loss of control, whereas the model exhibits unstable steer coupled to the unstable vehicle motion. Driver C does not lose control for any of the events, and critically, when the standard tuned model for driver F is evaluated using the speed input of driver C, it loses control multiple times (not shown). Figure 6(c) shows how the path compares between driver C and his model on the corner at 4.7 km; both tripped and untripped models show similar deviation behaviour to the actual driver. The tripped model has a steady-state offset, moving outside the lane, but this is due to its generic tendency to follow the path centreline in the approach to all corners, whereas the driver drifts to the left in anticipation.

These results give strong evidence that the tuned driver model is capable of capturing the innate skill level in the driving combination of speed and steer for these drivers, and indeed the model may also be capable of predicting driving response in an emergency. Note the records of the number of off-road events and average path tracking errors after each event, which are also given in Table 3. There is quantitative evidence here that driver C is consistently considerably more skilled than all the other drivers, that driver F is least skilled, and there also appears at least a loose correlation between lookahead distance T_p and driver skill. Note that T_p is unlikely to provide the measure of skill alone however; speed must also be considered. For example, driver K has the highest T_p coupled with a poor record of loss of control. His speed – seen in Figure 5(a) and later in Figure 7(b) – is generally the lowest of the five drivers examined here.

There does not appear to be a systematic link between the optimal K_{ug} and skill; rather this parameter simply provides an additional degree of freedom in the model, allowing it to match driver response more accurately. Tests carried out with optimisation of T_p alone showed that fitting accuracy (understandably) reduced.

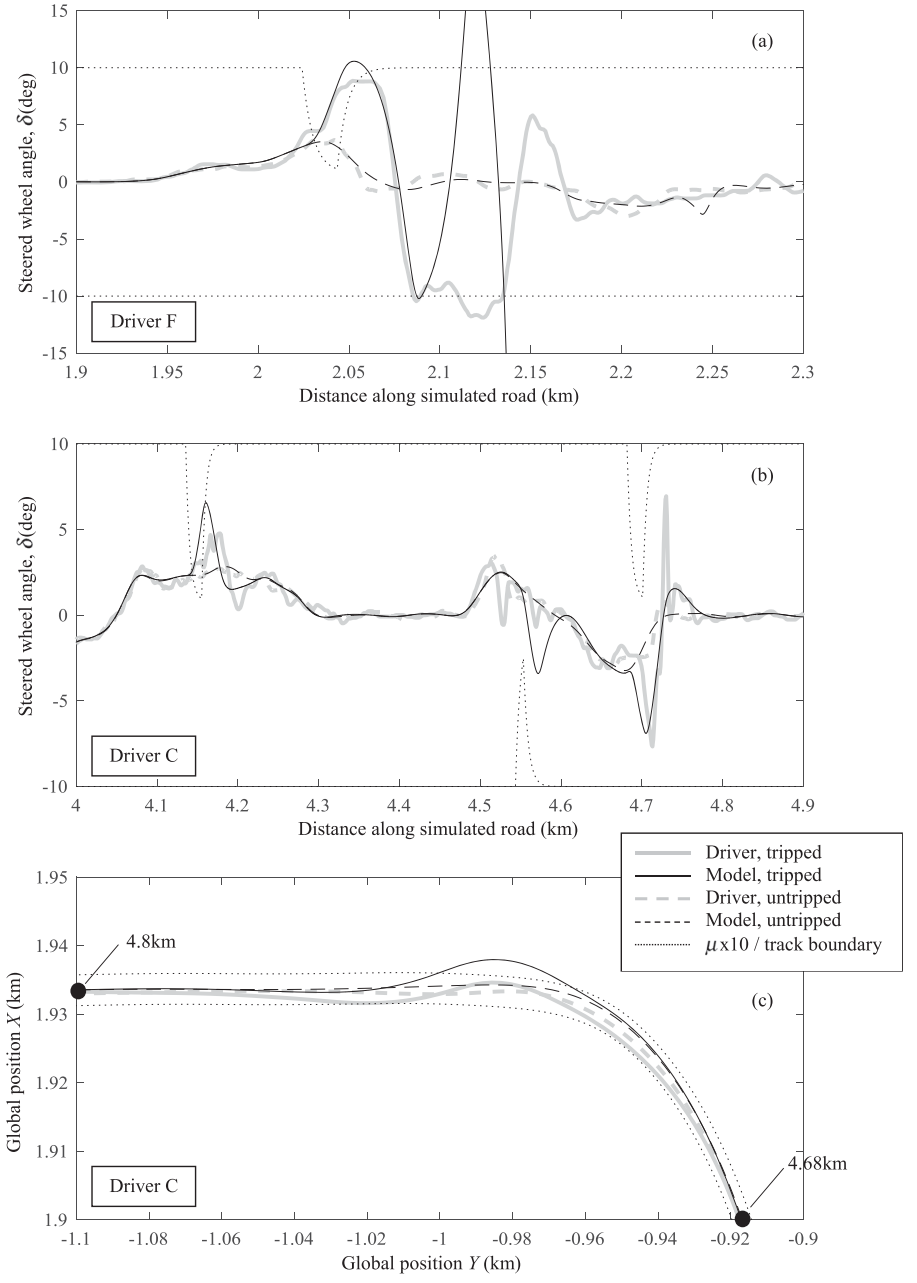

Figure 6. Comparing driver and driver model reactions with and without friction disturbance.

4. Unscented Kalman filter

To estimate and adapt T_p and K_{ug} in real time, a suitable observer can be used. This needs to incorporate both the vehicle and driver models as it must also estimate the driver–vehicle dynamic states. Kalman filters have widely been used in state estimation of nonlinear systems and have been applied for nonlinear system identification in [24,25]. The real-time

adaptation required here may be well suited to the application of either an extended Kalman filter (EKF) or an unscented Kalman filter (UKF) [24]. However, the standard EKF requires system Jacobians to be computed – a process which is not possible for the steer state of the driver model; the UKF is thus preferred as it identifies its own error statistics at each iteration, avoiding the need for Jacobians.

For a general nonlinear system and output model **f**, **h**, in continuous form, relating inputs **u** to measured outputs **y** under the influence of parameters θ, we can assume errors ω exist in the states, due to modelling error, and errors υ in the output are due to modelling error and noise on the measured outputs:

$$\dot{\mathbf{x}} = \mathbf{f}(\mathbf{x}, \mathbf{u}, \boldsymbol{\theta}) + \boldsymbol{\omega}, \tag{11}$$

$$\mathbf{y} = \mathbf{h}(\mathbf{x}, \mathbf{u}, \boldsymbol{\theta}) + \boldsymbol{\nu}. \tag{12}$$

By taking account of the magnitude of these errors using covariance estimates,

$$\mathbf{Q} = E(\boldsymbol{\omega}\boldsymbol{\omega}^{\mathrm{T}}), \quad \mathbf{R} = E(\boldsymbol{\nu}\boldsymbol{\nu}^{\mathrm{T}}) \tag{13}$$

the UKF computes state estimates $\hat{\mathbf{x}}$, along with estimates of state error covariance,

$$\mathbf{P} = E([\mathbf{x} - \hat{\mathbf{x}}][\mathbf{x} - \hat{\mathbf{x}}]^{\mathrm{T}}). \tag{14}$$

According to [26], this is done using a 'cloud' of $(2n+1)$ so-called sigma points $\boldsymbol{\chi}$ distributed around the nth-order state vector, at each instant k:

$$\begin{aligned} \boldsymbol{\chi}_{0k} &= \hat{\mathbf{x}}_k, \\ \boldsymbol{\chi}_{ik} &= \hat{\mathbf{x}}_k + \{\sqrt{(n+\kappa)\mathbf{P}_k}\}_i, \\ \boldsymbol{\chi}_{(i+n)k} &= \hat{\mathbf{x}}_k - \{\sqrt{(n+\kappa)\mathbf{P}_k}\}_i, \end{aligned} \tag{15}$$

where $\{\sqrt{(n+\kappa)\mathbf{P}_k}\}_i$ is the ith column of the matrix square root of $(n+\kappa)\mathbf{P}_k$, obtained using Cholesky decomposition. The sigma points are propagated using Euler integration

$$\boldsymbol{\chi}_{i(k+1)} = T\mathbf{f}(\boldsymbol{\chi}_{ik}, \mathbf{u}_k, \boldsymbol{\theta}) \tag{16}$$

and intermediate estimates for the propagated state and state error covariance matrix are computed by weighted averages:

$$\begin{aligned} \hat{\mathbf{x}}^*_{k+1} &= \sum_{i=0-2n} W_i \boldsymbol{\chi}_{i(k+1)}, \\ \mathbf{P}^*_{k+1} &= \sum_{i=0-2n} W_i \{\boldsymbol{\chi}_{i(k+1)} - \hat{\mathbf{x}}_{(k+1)}\}\{\boldsymbol{\chi}_{i(k+1)} - \hat{\mathbf{x}}_{(k+1)}\}^T + T\mathbf{Q}, \end{aligned} \tag{17}$$

with $W_0 = \kappa/(n+\kappa)$ and for all other i, $W_i = 1/2(n+\kappa)$.

Averaged estimates of the outputs are then obtained according to the output model:

$$\begin{aligned} \Upsilon_{i(k+1)} &= \mathbf{h}(\boldsymbol{\chi}_{ik}, \mathbf{u}_k, \boldsymbol{\theta}), \\ \hat{\mathbf{y}}_{k+1} &= \sum_{i=0-2n} W_i \Upsilon_{i(k+1)}. \end{aligned} \tag{18}$$

The UKF propagates output error covariance according to the transformed sigma points:

$$\mathbf{P}_{yy} = \sum_{i=0-2n} W_i \{\Upsilon_{i(k+1)} - \hat{\mathbf{y}}_{(k+1)}\}\{\Upsilon_{i(k+1)} - \hat{\mathbf{y}}_{(k+1)}\}^{\mathrm{T}} + \mathbf{R} \tag{19}$$

and uses this together with a cross-correlation estimate

$$\mathbf{P}_{xy} = \sum_{i=0-2n} W_i \{\boldsymbol{\chi}_{i(k+1)} - \hat{\mathbf{x}}_{(k+1)}\}\{\Upsilon_{i(k+1)} - \hat{\mathbf{y}}_{(k+1)}\}^{\mathrm{T}} \tag{20}$$

to find the Kalman gain at each discrete time step,

$$\mathbf{K}_{k+1} = \mathbf{P}_{xy}\mathbf{P}_{yy}^{-1}. \tag{21}$$

State and covariance estimates are then updated using the innovation sequence (the error between measured and estimated output),

$$\begin{aligned} \mathbf{P}_{k+1} &= \mathbf{P}^*_{k+1} - \mathbf{K}_{k+1}\mathbf{P}_{yy}\mathbf{K}^{\mathrm{T}}_{k+1}, \\ \hat{\mathbf{x}}_{k+1} &= \hat{\mathbf{x}}^*_{k+1} + \mathbf{K}_{k+1}(\mathbf{y}_{k+1} - \hat{\mathbf{y}}_{k+1}). \end{aligned} \tag{22}$$

To incorporate vehicle and driver models appropriately, Equations (8)–(10) are employed to form a subset of states

$$\mathbf{z} = [\delta, v, r, \psi, X, Y]^{\mathrm{T}}. \tag{23}$$

This is achieved in an obvious way by matching the time constant of the driver model with that of the filter, here $T = 0.01$ s, and considering Equation (8) in its equivalent continuous form as $\dot{\delta} = (K_{lat}T)d_L$.

Adaptation of the driver parameters is then achieved by expansion of the state set, to

$$\mathbf{x} = \begin{bmatrix} \mathbf{z} \\ T_p \\ K_{ug} \end{bmatrix}. \tag{24}$$

Of course, no 'model' exists for the parameter states, so

$$\begin{aligned} \dot{T}_p &= 0, \\ \dot{K}_{ug} &= 0 \end{aligned} \tag{25}$$

and the filter adapts the parameters through the assumption of non-zero modelling error on these additional states alone; set

$$\mathbf{Q} = \begin{bmatrix} \mathbf{0}_{6\times6} & \mathbf{0}_{6\times2} \\ \mathbf{0}_{2\times6} & \rho\mathbf{I}_{2\times2} \end{bmatrix} \tag{26}$$

The output, which will drive variation of the parameters, through the innovations, is the measured steer,

$$\mathbf{y} = \delta \tag{27}$$

and its error covariance estimate can be set appropriately, according to our experience with the optimised driver model in Section 3,

$$\mathbf{R} = 10^{-5}. \tag{28}$$

The filter can now operate using measured steer, inputs of measured forward speed and known path, and a suitable initial condition set,

$$\mathbf{P}_0 = \mathbf{Q}, \quad \mathbf{x}_0 = [\delta_0, 0, 0, \psi_0, X_0, Y_0, T_{p0}, K_{ug0}]^{\mathrm{T}}. \tag{29}$$

A small set of sigma points is effective, so set $\kappa = 1$, and the only remaining tunable parameter is the assumed parameter error magnitude ρ. The effect of ρ is explored in [24]; essentially it governs the speed of variation of the parameter states and can be set in steps of order of magnitude. For the tests in the following section, $\rho = 10^{-3}$ is the limiting high value at which the filter can become unstable, $\rho = 10^{-8}$ causes the parameter adaptation to be too slow, so results were collected using $\rho = 10^{-5}$.

Regardless of ρ setting the resulting filter is computationally very efficient. At the sampling rate used here, 193 s of data is processed in 7.5 s using Matlab R2016a on a desktop PC with 16 GB RAM and Intel i7 3.6 GHz processor.

5. Characterisation results and robustness

The UKF drives estimates of the parameter states T_p and K_{ug} to improve the estimate of the steer output. This can be demonstrated by comparing the filter estimate of steer with that from the model using optimised best-fit fixed values of T_p and K_{ug}. Table 4 gives the optimised parameters along with comparisons of mean square steer error for both simulator and open road experiments. Figure 7(a) illustrates how the steer accuracy is improved by the operation of the filter. The remainder of Figure 7 then shows how speed and the

Table 4. Optimised models and UKF performance comparisons in simulation and open road tests.

		Driver identifier				
		B	C	F	K	T
Simulation tests	T_p (s), $K_{ug}/10^3$ (rad/g)	0.81, 0.3	0.92, 0.8	0.56, −1.3	0.97, −0.4	0.83, 0.1
	δ error covariance, fixed parameters ($\times10^{-6}$)	23.4	24.1	44.4	25.4	18.0
	δ error covariance, UKF parameters ($\times10^{-6}$)	16.0	19.0	27.0	18.2	25.8
Open road tests	T_p (s), $K_{ug}/10^3$ (rad/g)	1.02, 1.77	0.94, 2.97	0.91, 4.04	1.12, 3.13	1.13, 1.89
	δ error covariance, fixed parameters ($\times10^{-6}$)	7.68	11.63	10.78	7.35	10.16
	δ error covariance, UKF parameters ($\times10^{-6}$)	5.87	8.89	7.21	6.23	8.59

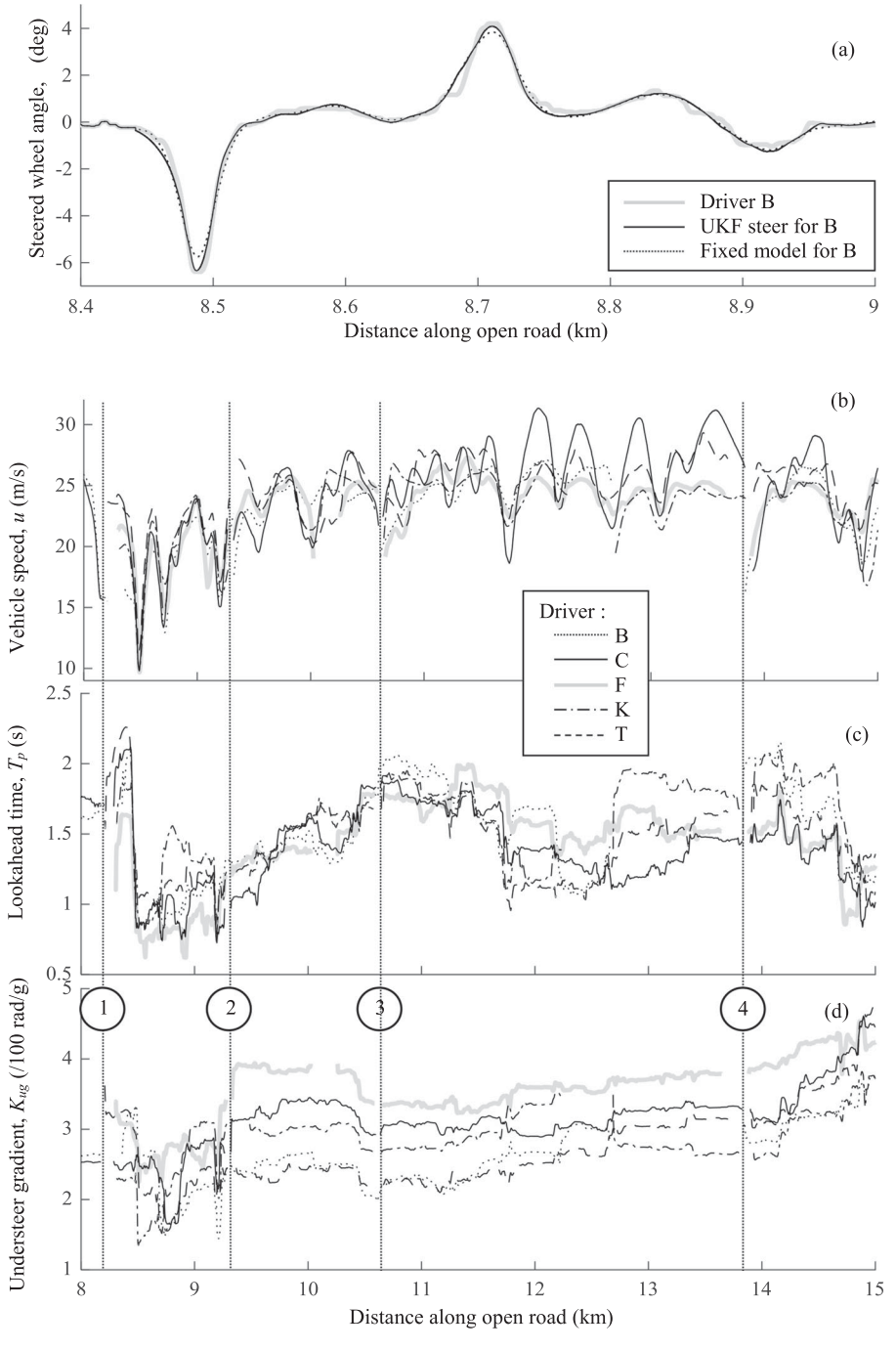

Figure 7. Variation of steer and characterising parameters under the UKF.

estimated parameter states from the filter vary, over 7 km of free driving. The domain here is the distance along the reference path, so driver behaviour can be compared on the same sections of road. The road within villages – that may interrupt the driving 'flow' – has been removed and each village is annotated by a circled number.

First, note how the road topography can have a strong influence on driving behaviour; the distinctly uniform increase in T_p between villages 1 and 3 is initiated by a pair of slow corners around 8.4 km. It is interesting that all the drivers also gradually increase their average speed between these two points – a trend apparently uninterrupted by village 2. We can see that lookahead *time* T_p increases with speed. This is almost certainly due to modelling simplicity; the correlated behaviour suggests lookahead *distance* does not simply scale with speed. Note how reactive the filter is; with $\rho = 10^{-5}$ we can clearly see large changes in both parameters over the course of single corner events. The steer accuracy figures in Table 4 clearly show that these parameter changes are successful in continuously adapting the driver model to better fit the instantaneous steer behaviour.

The steady-state differences between drivers remains identifiable on the open road, though T_p for driver C is relatively low; real track width varies, but at around 3 m is significantly lower than the simulated track, yet for most of the observed sections driver F has lower T_p than driver K. We also see evidence of apparently random changes – e.g. between 11 and 12 km, where driver F has uncharacteristically high T_p and around 11.8 km, where driver B increases his lookahead while all other drivers decrease theirs. Driver mood and concentration vary over time and this may explain parameter variations such as these – further research will be needed to formally correlate skill or concentration to the parameters. Some model developments (for example in altering the speed dependence of T_p) may make this task easier. It will also be valuable to combine an adaptive longitudinal model with the steer model; note how significant the difference in average speed and variance in speed is, between drivers C, F and K in Figure 7(b). There are obvious correlations between speed and risk-taking in driver behaviour, so a combination of UKF adapted parameters in a future combined model should have the capacity to more strongly characterise overall driving behaviour.

Finally, it is important to consider the robustness properties of the new filter. In addition to the reference path, only steer and speed are continuously provided as inputs, both of which are easily available in the current vehicle CAN. However, each initiation of the filter also needs instantaneous vehicle position $[X_{G0}, Y_{G0}]$ and orientation ψ_0. These may be known, but will rely on the accuracy of the GPS and orientation sensors available on the vehicle, which may not be good. Thankfully the filter is robust to large errors in these initial conditions; Figure 8(a) shows a close-up of the start of the path taken by the filter when it is deliberately given a [+8 m, +8 m] error in initial position, and a −50° error in ψ. Very sharp positive steer is first seen at the start of plot (b), and over the next few minutes of filter operation the evident phase errors in steer are gradually compensated and removed. Figure 8(c) shows the difference between actual vehicle position and that of the filter *along* the track, illustrating a steady reduction of error over time. The filter effectively corrects the initialisation error to 'catch up with' the test vehicle.

As with any driver model, the UKF must have knowledge of the path ahead. On most single carriageway roads, this information is available from existing digitised road maps. However it will still be necessary to compensate the filter to manage events where the path ahead is unpredictable or becomes invalid, such as a fork in the road, a T junction or simply overtaking a cyclist. Although we do not consider such advanced detail here, it should be possible to make retrospective corrections to the filter, e.g. by placing limits on the expected innovations (errors between modelled and measured steer) that are allowed to modify the parameter states.

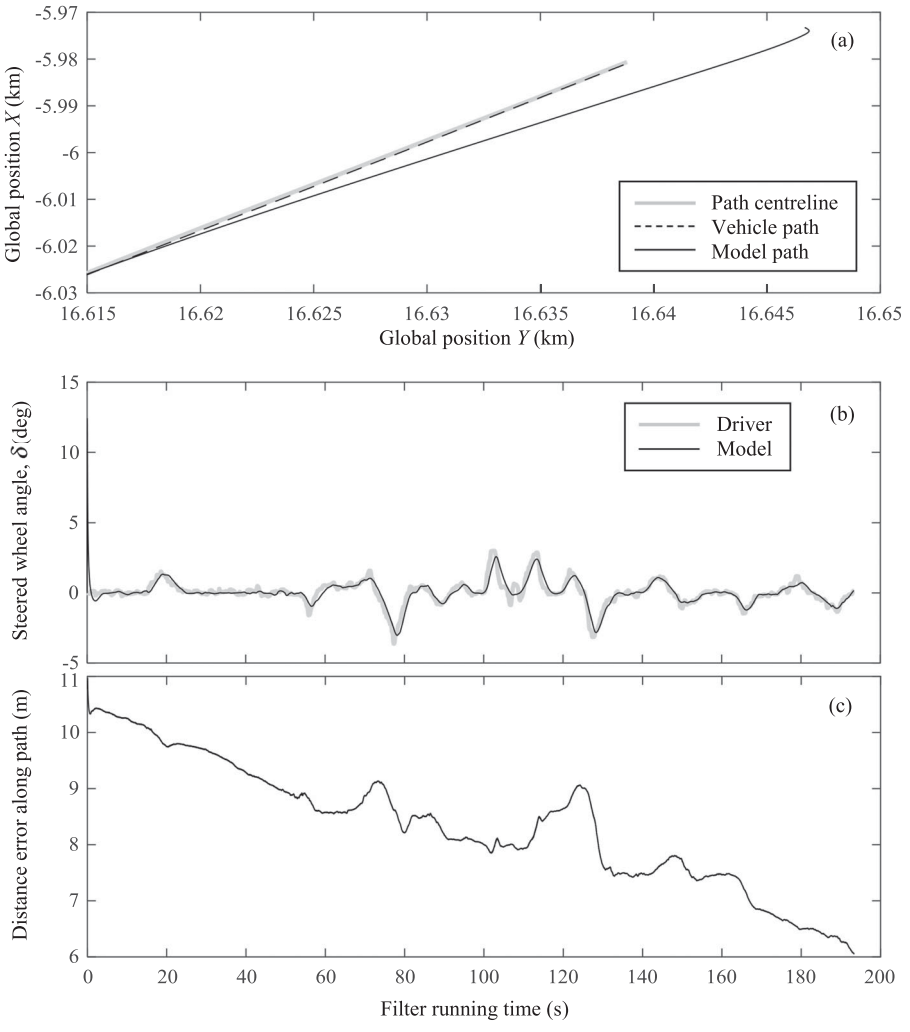

Figure 8. Robustness of the UKF to errors in initial conditions.

6. Conclusions

A simple but effective lateral driver model is presented, which depends on only three parameters. By tuning two of these, it is shown that the model is capable of accurately replicating normal steering behaviour on open single carriageway roads. Further, the parameters can be tuned to map differences between the steering behaviour of five test drivers, in experiments on a motion simulator and also on the public road.

In combination with a single-track vehicle handling model, the steer model has been successfully integrated into an UKF in order to estimate the characterising parameters in real time; this is an entirely novel application. The resulting filter provides parameter variations which are demonstrated to fit individual driver steer behaviour more accurately than an optimised fixed parameter model, in both tested environments. It depends on the known road geometry and available CAN measurements of steer and speed, with actual

vehicle position and orientation only required as initial conditions. Moreover, a robustness study has demonstrated that the filter is capable of rejecting significant errors in these initial conditions.

The filter is fast, running 25 times faster than real time on the PC used for the data analysis here; it is therefore immediately practicable. Although further research is needed to correlate driver concentration, mood and/or skill to the identified parameters, this research shows exciting prospects for the real time use of an adaptable driver model filter in a range of potential applications, including

- Prediction of driver concentration, state of awareness and skill, to support ADAS.
- Adaptation of automated driving style to the driving style of individual drivers, in future autonomous vehicles.
- Quantification of insurance risk.

Acknowledgements

The author gratefully acknowledges the support of Jaguar LandRover for the provision of the test vehicle used in this study and for access to required supporting vehicle and CAN data.

Disclosure statement

No potential conflict of interest was reported by the author.

References

[1] MacAdam CC. Application of an optimal preview control for simulation of closed-loop automobile driving. IEEE Trans Syst Man Cybern. 1981;11:393–399.
[2] Sharp RS, Casanova D, Symonds P. A mathematical model for driver steering control, with design, tuning and performance results. Veh Syst Dyn. 2000;33:289–326.
[3] Ungoren AY, Peng H. An adaptive lateral preview driver model. Veh Syst Dyn. 2005;43:245–259.
[4] Keen SD, Cole DJ. Application of time-variant predictive control to modelling driver steering skill. Veh Syst Dyn. 2011;49(4):527–559.
[5] Cole DJ. A path-following driver–vehicle model with neuromuscular dynamics, including measured and simulated responses to a step in steering angle overlay. Veh Syst Dyn. 2012;50(4):573–596.
[6] Bi L, Wang M, Wang C, et al. Development of a driver lateral control model by integrating neuromuscular dynamics into the queuing network-based driver model. IEEE Trans Intell Transp Syst. 2015;16(5):2479–2486.
[7] Flad M, Trautmann C, Diehm G, et al. Experimental validation of a driver steering model based on switching of driver specific primitives. Proceeding of the 2013 IEEE International Conference on Systems, Man, and Cybernetics; 2013 Oct 13–16; Manchester, UK; 2013. p. 214–220.
[8] Nash CJ, Cole DJ. Modelling the influence of sensory dynamics on linear and nonlinear driver steering control. Veh Syst Dyn. 2017;56(5):1–30.
[9] Saigo S, Raksincharoensak P, Nagai M. Estimation of driving performance level using longitudinal and lateral driver models. 7th IFAC Symposium on Advances in Automotive Control, AAC 2013, IFAC Proceedings Volumes (IFAC-PapersOnline); Tokyo. 2013; 7(1):145–150.
[10] Erséus A, Drugge L, Trigell AS. A path tracking driver model with representation of driving skill. Int J Veh Syst Model Test. 2011;6(2):145–186.
[11] Moon C, Seibum B. A driver model for vehicle lateral dynamics. Int J Veh Des. 2011;56(1–4):49–80.

[12] Schnelle S, Wang J, Su H, et al. A driver steering model with personalized desired path generation. IEEE Trans Syst Man Cybern: Syst. 2017;47(1):111–120.
[13] Ostapczuk M, Joseph R, Pufal J, et al. Validation of the German version of the driver skill inventory (DSI) and the driver social desirability scales (DSDS). Transp Res Part F: Traffic Psychol Behav. 2017;45:169–182.
[14] Wallace B, Goubran R, Knoefel F, et al. Driver unique acceleration behaviours and stability over two years. Proceedings of the 2016 IEEE International Congress on Big Data; 2016 Oct 6; Bethesda, MD; 2016. p. 230–235.
[15] Carmona J, Garcia F, Martin D, et al. Data fusion for driver behaviour analysis. Sensors. 2015;15(10):25968–25991.
[16] Chu D, Deng Z, He Y, et al. Curve speed model for driver assistance based on driving style classification. IET Intel Transport Syst. 2017;11(8):501–510.
[17] Tokutake H, Sugimoto Y, Shirakata T. Real-time identification method of driver model with steering manipulation. Veh Syst Dyn. 2013;51(1):109–121.
[18] Hosseini S, Köroglu H, Sjöberg J. Estimation of parameters and delay in driver models using L1-regularization. Proceedings of the European Control Conference (ECC); 2016 Jun 29–Jul 1; Aalborg, Denmark; 2016. p. 945–950.
[19] Mihaly A, Gaspar P. Identification of a linear driver model based on simulator experiments. Proceedings of the 9th IEEE International Symposium on Applied Computational Intelligence and Informatics; 2014 May 15–17; Timisoara, Romania; 2014. p. 13–18.
[20] Best MC. A simple realistic driver model. Proceedings of the 11th International Symposium on Advanced Vehicle Control (AVEC); 2012 Sept 9–12; Seoul, Korea.
[21] Johns TA, Cole DJ. Measurement and mathematical model of a driver's intermittent compensatory steering control. Veh Syst Dyn. 2015;53(12):1811–1829.
[22] Gillespie TD. Fundamentals of vehicle dynamics. Warrendale (PA): SAE International; 1992.
[23] Newton A, Best MC. The influence of motion on handling dynamics analysis in full vehicle simulators. Proceedings of the 8th International Symposium on Advanced Vehicle Control (AVEC); 2006 Aug 20–24; Taipei, Taiwan.
[24] Bogdanski K, Best MC. Kalman and particle filtering methods for full vehicle and tyre identification. Veh Syst Dyn. 2017. DOI:10.1080/00423114.2017.1337914
[25] Bogdanski K, Best MC. A new structure for non-linear black-box system identification using the extended Kalman filter. Proc IMechE Part D: J Automob Eng. 2017. DOI:10.1177/0954407017692219
[26] Julier SJ, Uhlmann JK. A new extension of the Kalman filter to nonlinear systems. Proceedings of the AeroSense: 11th International Symposium on Aerospace/Defense Sensing, Simulations and Controls; 1997 Apr; Orlando, FL; 1997. p. 182–193.

Appendix. Driver model implementation in Matlab/Simulink

The driver model can easily be implemented in Simulink with the layout of Figure A1, using a Matlab function block, the code for which is given below. The function block must be configured as a discrete block with update rate set, e.g. $T = 0.01$ as used here, and the same rate is used for the delays. Many of the function inputs are pre-calculated parameters set as follows. (NB: see the Simulink Model Explorer to set the discrete block configuration, and to set function inputs as parameters.)

`Kug`, **`Klat`**, **`Tp`**, **`L`**: Scalar driver model gains, and vehicle wheelbase
`SLset`: $n \times 2$ array of global (X,Y) position vectors of start points of the n line segments defining the path
`rLhatset`: $n \times 2$ array of unit tangential vectors giving the direction of the n line segments
`nLhatset`: $n \times 2$ array of unit normal vectors giving the normal to each of the n line segments
`rLmagset`: $n \times 1$ vector of magnitudes of $\mathbf{r}_L$ (distances in m) of each of the n line segments

```
function
[steernext,inext] = DRIVER(steer,x,i,Kug,L,Klat,Tp,SLset,
rLhatset,nLhatset,rLmagset)
```

```
% Extract variables from state vector :
psi = x(1);
G = x(2:3);
u = x(4);
g = 9.81;
% Find P :
tGhat = [cos(psi); sin(psi)];
R = (L+Kug*u*u/g)/steer;
if abs(steer) < 1e-6
  % Assume a straight path if steer is very small
  P = G+u*Tp*tGhat;
else
  theta = u*Tp/R;
  nGhat = [-tGhat(2); tGhat(1)];
  rotmat = [cos(theta), -sin(theta); sin(theta), cos(theta)];
  P = G+R*nGhat - R*rotmat*nGhat;
end
% Manage line segments (increase i if required)
Sp = P-SLset(:,i);
si = Sp'*rLhatset(:,i);
while si > rLmagset(i)
  % step forward to next track segment :
  i = i+1;
  Sp = P-SLset(:,i);
  si = Sp'*rLhatset(:,i);
end
d = Sp'*nLhatset(:,i);
inext = i;
% Apply steer control
steernext = steer - Klat*d;
```

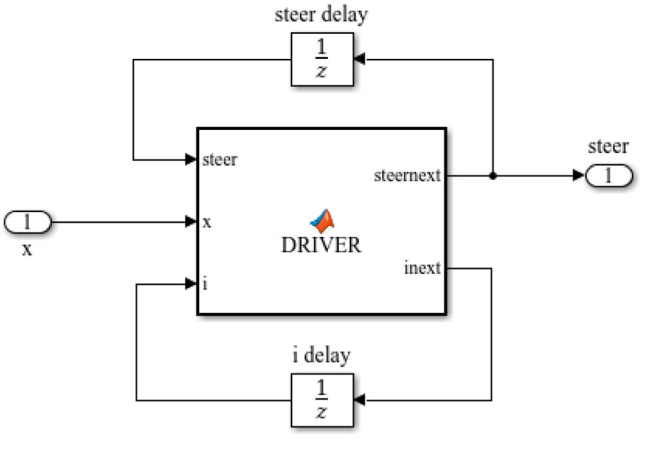

Figure A1. Simulink layout for driver model implementation.